GEOPHYSICS, VOL. 77, NO. 3 (MAY-JUNE 2012); P. H33–H44, 9 FIGS., 1 TABLE.
10.1190/GEO2011-0100.1

Coupling of dielectric mixing models with full-wave ground-penetrating radar signal inversion for sandy-soil-moisture estimation

Anh Phuong Tran[1], Mohammad Reza Mahmoudzadeh Ardekani[1], and Sébastien Lambot[1]

ABSTRACT

We coupled dielectric mixing models with a full-wave ground-penetrating-radar (GPR) model to estimate the soil water content by inversion. Two mixing models were taken into account in this study, namely, a power law model and the Wang and Schmugge model. With this combination, we could account for the frequency dependence of the dielectric permittivity and apparent conductivity in the inverse algorithm and directly estimate the soil water content without using an empirical petrophysical formula or a priori knowledge on soil porosity. The approach was validated by a series of experiments with sandy soil in controlled laboratory conditions. The results showed that the performance of our approach is better than the common approach, which assumes a linear dependence of apparent conductivity on frequency and uses Topp's equation to transform permittivity to water content. GPR data were perfectly reproduced in the time and frequency domains, leading to very accurate water-content estimates with an average absolute error of less than 0.013 cm^3/cm^3. However, the accuracy was reduced as the water content increased. Sensitivity analysis indicated that the Green's function was most sensitive to the water content and sand-layer thickness but much less so with DC conductivity. The results also revealed that as the frequency increased, although the permittivity was nearly constant, the apparent electrical conductivity and the attenuation increased remarkably, especially for wet sands due to dielectric losses. The successful validation of the proposed approach opens a promising avenue of development to use dielectric mixing models for soil-moisture mapping from GPR measurements.

INTRODUCTION

Soil moisture is one of the most important pieces of information for agricultural, ecological, hydrological, and meteorological research and applications (Huisman et al., 2003; Lambot et al., 2006; Vereecken et al., 2008). Thus, for sustainable agricultural and environmental management and accurate hydrometeorological predictions, there is an urgent demand to know this information in time and space. With advances in instrumentation and electronics over the past 20 years, there have been various techniques invented to estimate soil water content across a range of scales (Robinson et al., 2008). Although the contact-based methods like destructive sampling, capacitance sensors, or time-domain reflectometry (TDR) are usually used to provide high-resolution information on soil moisture at the point scale, remote sensing techniques like airborne and spaceborne passive microwave radiometry and active radar systems are a good choice for retrieving soil water content at the large scale (Weihermüller et al., 2007). However, at the field or small catchment scale, the data based on sparse points or coarse remote-sensing measurements cannot provide a quantitatively accurate soil-moisture map. In that sense, ground-penetrating radar (GPR) has emerged as a promising noninvasive tool for soil-moisture investigation at the intermediate scale (Lambot et al., 2006; Strobbia and Cassiani, 2007; Slob et al., 2010).

Based on the domination of the water permittivity over the other components in the soil mixtures, several approaches have been proposed to interpret water content from GPR backscattered signals. Huisman et al. (2003) provide an excellent review of these approaches. In brief, these approaches can be divided into three groups. The first one is the most simple and earliest method that derives the permittivity from the analysis of the propagation velocity of the ground waves (Greaves et al., 1996; Huisman

Manuscript received by the Editor 10 March 2011; revised manuscript received 25 January 2012; published online 9 April 2012.
[1]Université Catholique de Louvain, Earth and Life Institute, Louvain-la-Neuve, Belgium. E-mail: phuong.tran@uclouvain.be; mohammad.mahmoudzadeh@uclouvain.be; sebastien.lambot@uclouvain.be.

et al., 2001; Galagedara et al., 2005) based on multiple-offset GPR acquisition geometry. In several special cases, for example, when the water-soaked upper part of the subsurface after rainfall or irrigation generates a low-velocity waveguide that traps the electromagnetic waves, the application of the ground-wave method is not effective any more. In those cases, an inverse technique of the dispersed waveforms can be used to retrieve the permittivity and thickness of these layers (van der Kruk et al., 2010). The second approach, known as the surface reflection coefficient method, computes the dielectric permittivity from the Fresnel reflection coefficient, defined by the ratio between the reflection amplitudes obtained at the soil surface and for a perfect electrical conductor (Chanzy et al., 1996; Redman et al., 2002; Lambot et al., 2006). For thin-layer reflectors, Gregoire and Hollender (2004) compare the spectral ratio between measured reflected wavelets and a reference wavelet to predict the dielectric permittivity and layer thickness by minimizing the discrepancy between modeled and measured GPR data. The inversion works well, provided that the ratio of the dominant wavelength to the layer thickness is lower than four. Recently, several authors have attempted to apply the amplitude-variation-with-offset (AVO) dependent reflectivity analysis (Bradford and Deeds, 2006) or dispersive amplitude and phase versus offset (DAPVO) (Deparis and Garambois, 2009) for thin-bed characterization based on common-midpoint (CMP) geometry acquisition. The third approach, developed by Lambot et al. (2004c, 2007), determines the soil properties based on full-wave inversion of GPR signals in either frequency or time domains for an off-ground, zero-offset antenna configuration. The radar-antenna-subsurface system is modeled by a linear transfer function system and exact solution of Maxwell's equations for wave propagation in planar layered media. The geophysical properties of each layer can be found using a global optimization algorithm. The advantages of this approach over the two first methods are that (1) all information contained in the radar data is used in the inversion process and (2) all antenna effects, including antenna-soil interactions and spherical divergence in wave propagation, are also taken into account.

In GPR applications, the two main geophysical properties are permittivity and conductivity, which are frequency-dependent quantities (Saarenketo, 1998; Deparis and Garambois, 2009). To obtain accurate and realistic values of these properties, this dependence should be included in the inverse model. However, there have not been many studies investigating the problem so far, especially in the GPR field (West et al., 2003; Lambot et al., 2005). Saarenketo (1998) uses a vector network analyzer (VNA) to investigate the variation of the electrical properties of silt and clay soils with different densities and water contents over the GPR frequency range from 30 MHz to 3 GHz. Gregoire and Hollender (2004) and Deparis and Garambois (2009) employ the Jonscher law to formulate the relationship between the complex effective dielectric permittivity and the frequency. Lambot et al. (2005) assume an independence of the permittivity and a locally linear dependence of the apparent electrical conductivity on the frequency for a sandy soil in the range of 1–3 GHz for the full-wave inversion of off-ground, zero-offset GPR data. This assumption works well for the selected frequency range. However, as they mention, when the frequency range extends more widely and water content increases, a more appropriate model would be required.

The key step in estimating soil moisture of the subsurface from GPR signals is the transformation of the geophysical properties into water content, which is typically done by using petrophysical relationships. Generally, two main approaches to develop these relationships are used. The first approach uses empirical equations to relate water content to permittivity based on measurements with different soil types (Topp et al., 1980). The second approach, more advanced, predicts the water content from dielectric mixing models of soils. According to this approach, soil permittivity is expressed by the permittivities of air, water, and soil particles and their volume fractions. Therefore, given the permittivities and portions of other components, water content can be determined (Wang and Schmugge, 1980; Dobson et al., 1985; Heimovaara, 1994). Compared with the empirical formulas, the dielectric mixing models take into account the composition of soil materials and thus are expected to better predict the water content. However, a drawback of this approach is that it requires a priori knowledge of the porosity of the soil material and permittivities of the individual constituents (Lesmes and Friedman, 2005). Detailed reviews on the petrophysical relationships are found in the works of Robinson et al. (2003) and Lesmes and Friedman (2005).

In this paper, we propose an approach that integrates different mixing models of the effective complex permittivity into the full-wave inversion of GPR signals to estimate the water content of sandy soil. Instead of estimating the water content from the dielectric permittivity, we can derive directly the water content from inversion of GPR signals. The frequency dependence of the sand permittivity and apparent conductivity are accounted for via the permittivity and conductivity of water component, which varies with frequency by the Debye equation. By regarding soil porosity as an optimized variable, our approach also does not need to a priori determine this value when the dielectric mixing models are used. Our approach is validated by controlled laboratory experiments with a sandy soil subject to various water contents. Obtained results are compared with each other and with those of Lambot et al.'s (2005) approach to select the best model for our problem. Uncertainty analysis of the electrical properties and sensitivity analysis of the model signal with the optimized parameters are also presented.

THEORY

Forward modeling

For transmitting and receiving the GPR signals, we adopt a measurement system as described in the work of Lambot et al. (2004c). The system contains a VNA and an off-ground ultrawideband zero-offset horn antenna connected by a 50-Ω-impedance coaxial cable. The distance from the phase center of the antenna to the medium should be large enough so that the far-field radar model can be applied (typically larger than the dimension of the antenna) but should be minimized to reduce losses by spherical divergence (to maximize signal-to-noise ratio [S/N]). For this configuration, the antenna can be modeled using the following equation in the frequency domain (Lambot et al., 2004c):

$$S_{11} = \frac{b(\omega)}{a(\omega)} = H_i(\omega) + \frac{H(\omega)G_{xx}^{\uparrow}(\omega)}{1 - H_f(\omega)G_{xx}^{\uparrow}(\omega)}, \qquad (1)$$

in which ω is the angular frequency; $b(\omega)$ and $a(\omega)$ are received and transmitted waves at the VNA calibration plane, respectively; $H_i(\omega)$ is the global reflection coefficient of the antenna for the incident field; $H(\omega)$ is the global transmitting-receiving coefficient;

$H_f(\omega)$ is the global reflection coefficient of the antenna for the scattered field; and $G_{xx}^{\uparrow}(\omega)$ is the Green's function, which is an exact solution of Maxwell's equations for electromagnetic wave propagation in planar layered media. The Green's function can be mathematically obtained by solving Maxwell's equations given the frequency, antenna height, thickness, effective permittivity, and apparent conductivity of each layer. A fast procedure is used to calculate the spatial-domain Green's function from its spectral counterpart (Lambot et al., 2007).

The characteristic antenna properties $H(\omega)$, $H_i(\omega)$, and $H_f(\omega)$ characterizing the antenna can be estimated for the entire frequency range by solving equation 1 based on different configurations, which, in our study, are antenna heights above a copper plane as an infinite perfect electrical conductor (PEC).

Mixing models

To include the frequency dependence of the permittivity and apparent conductivity, our research used the mixing models of the effective complex permittivity instead of the dielectric permittivity as commonly adopted approaches. Two models were taken into account in this research: a power law model and the four-component mixing model of Wang and Schmugge (1980). The power law model is a family of equations that relates a certain power of the effective complex permittivity ε_e of the mixture with the same power of its components:

$$\varepsilon_e^{\gamma} = \theta\varepsilon_w^{\gamma} + (\phi-\theta)\varepsilon_a^{\gamma} + (1-\phi)\varepsilon_s^{\gamma}, \tag{2}$$

in which γ is the empirical coefficient of the equation that depends on the soil structure and its orientation with respect to the electromagnetic field. Different authors use different coefficients that provide the best fit to their data (Looyenga, 1965; Dobson et al., 1985). In this paper, we use the most popular coefficient in soil science, $\gamma = 0.5$, which was widely known as the complex refractive index model (CRIM). CRIM was also confirmed by Shutko and Reutov (1982), Roth et al. (1990), and Gorriti (2004) as the most suitable power law model. The porosity and volumetric water content of soil are ϕ and θ, respectively; ε_a, ε_w, and ε_s are the permittivities of air, water, and soil particles in which permittivity of water is a function of frequency, expressed by the Debye equation (Debye, 1929):

$$\varepsilon_w = \varepsilon_\infty + \frac{\varepsilon_{sp}-\varepsilon_\infty}{1+j\omega\tau} - j\frac{\sigma_{\mathrm{DC}}}{\omega\varepsilon_0}, \tag{3}$$

where ω is the angular frequency and σ_{DC} is the direct-current (DC) conductivity (ionic conductivity) of water in the soil pores. It is worth noting that the apparent conductivity becomes the direct-current conductivity as the frequency is equal to zero; ε_0 is the dielectric permittivity of the free space ($\varepsilon_0 = 8.8542\times10^{-12}$ F/m); and ε_{sp} is the static permittivity of pure water, which was determined by Lane and Saxton (1952) to be 4.9. The dependence of the water permittivity on temperature T is accounted for via the relative permittivity at infinite frequency ε_∞ (Klein and Swift, 1977), in which

$$\varepsilon_\infty = 88.045 - 0.4147T + 6.295\times10^{-4}T^2 + 1.075\times10^{-5}T^3, \tag{4}$$

and relaxation time τ (Stogryn, 1970), in which

$$\tau = \frac{1}{2\pi}(1.1109\times10^{-10} - 3.824\times10^{-12}T + 6.938\times10^{-14}T^2 - 5.096\times10^{-16}T^3). \tag{5}$$

In contrast to the power-law model that considers only three components of soil materials, the mixing model of Wang and Schmugge (1980) accounts for four components. In addition to the free water, soil matrix, and air, the bound-water component, which is tightly bound to the soil-particle surface, is included in the model. Because it is nearer to the soil-particle surface, the rotation of the bound-water molecules is more difficult than the free water, leading to smaller dielectric permittivity and lowering their relaxation frequency (West et al., 2003). Investigating the relationship between the complex dielectric permittivity and soil moisture, West et al. (2003) find that this relationship changes after the soil moisture reaches a transition point. Consequently, they assume that the transition moisture is a division between the bound- and free-water components. Two mixing formulas to calculate the effective complex permittivity were also developed, depending on whether the soil moisture is greater or lower than the transition moisture. In addition, due to the fact that the contacting area between water and soil particles is inversely proportional to the grain size, a clay soil has a higher bound-water content and therefore lower permittivity than a sandy soil. This dependence of the dielectric permittivity on the soil type was indirectly taken into account via the empirical relationships between the transition moisture and the wilting-point moisture, which is a function of the sand and clay content. The following equations present the main ideas of Wang and Schmugge's (1980) soil-mixing model:

$$\varepsilon_e = \theta\varepsilon_x + (\phi-\theta)\varepsilon_a + (1-\phi)\varepsilon_s, \quad \text{for } \theta \le \theta_t, \tag{6}$$

with $\varepsilon_x = \varepsilon_i + (\varepsilon_w - \varepsilon_i)\frac{\theta}{\theta_t}\zeta$, and

$$\varepsilon_e = \theta_t\varepsilon_x + (\theta-\theta_t)\varepsilon_w + (\phi-\theta)\varepsilon_a + (1-\phi)\varepsilon_s, \quad \text{for } \theta > \theta_t, \tag{7}$$

with $\varepsilon_x = \varepsilon_i + (\varepsilon_w - \varepsilon_i)\zeta$, where ε_x stands for the permittivity of the initially absorbed water and ε_i is the permittivity of the bound water. If assuming that water present around sand particles is bound in a monomolecular layer, we can consider the dielectric permittivity of bound water to be equal to that of ice (about 3.2), although their structures are not the same (Dirksen and Dasberg, 1993; Saarenketo, 1998; Hilhorst et al., 2001; Woodhead et al., 2003). The wilting point θ_p, transition moisture θ_t, and free adjustable parameter ζ are estimated from the sand and clay contents as follows:

$$\theta_p = 0.068 - 0.00064S + 0.0048C, \tag{8}$$

$$\theta_t = 0.49\theta_p + 0.165, \tag{9}$$

$$\zeta = -0.57\theta_p + 0.481, \tag{10}$$

where S and C, respectively, are percentages of sand and clay in the soil materials. Because we worked only with the sandy soil in this study, S and C are equal to 100% and 0%, respectively.

Parameter estimation

The water content of the soil medium is directly obtained by an inverse modeling procedure in the frequency domain, as shown in Figure 1. Besides the water content, the unknown parameter vector **b** also contains the other variables, including the sand porosity ϕ, direct-current conductivity of the water in the sand pore (σ_{DC}), and thickness of the sand medium above the PEC (h). The flowchart in Figure 1 begins with the estimation of the Green's function from the measured reflectivity $S_{11}(\omega)$ by using equation 1. Next, the frequency-dependent apparent conductivity and dielectric permittivity are calculated by using the Debye equation 3 and mixing models CRIM (equation 2) or the Wang and Schmugge (1980) model (equations 6 and 7) given parameter vector **b**. To estimate the modeled Green's function, our experimental configuration is simulated by a three-layered medium (the air, sand, and PEC). The air layer has electric properties equal to those of the free space ($\varepsilon_r = 1$, $\sigma = 0$ S/m) and a thickness determined as the distance from the virtual source point to the soil surface. The PEC layer, which is the lower half-space in our model, has infinite thickness, infinite conductivity, and a relative permittivity of one. Based on this conceptual configuration, the modeled Green's function can then be analytically estimated using the transverse electric and magnetic global reflection coefficients in the spectral domain (Lambot et al., 2004c, 2007). The difference between the modeled and measured Green's functions is described by an objective function that is formulated in the least-squares sense as

$$\Phi(\mathbf{b}) = |\mathbf{G}_{\mathbf{xx}}^{\uparrow*} - \mathbf{G}_{\mathbf{xx}}^{\uparrow}|^T |\mathbf{G}_{\mathbf{xx}}^{\uparrow*} - \mathbf{G}_{\mathbf{xx}}^{\uparrow}| = \mathbf{e}^T\mathbf{e}, \qquad (11)$$

where $\mathbf{G}_{\mathbf{xx}}^{\uparrow*} = G_{xx}^{\uparrow*}(\omega)$ and $\mathbf{G}_{\mathbf{xx}}^{\uparrow} = G_{xx}^{\uparrow}(\mathbf{b}, \omega)$ are the measured and simulated complex Green's function vectors; **e** represents the difference between the modeled and measured Green's functions or the residual vector; and superscript T represents the complex conjugate transpose operator. Parameter vector **b** is determined at the point where the objective function 11 reaches its global minimum. For this nonlinear inverse problems, we followed the approach of Lambot et al. (2004c), who use the global multilevel coordinate search algorithm proposed by Huyer and Neumaier (1999) combined sequentially with the Nelder-Mead simplex algorithm given by Nelder and Mead (1965) to search for the optimal parameters. The optimization parameter space is ($0.025 < \theta < 0.3$ cm^3/cm^3; $0.3 < \phi < 0.5$; $10^{-4} < \sigma_{\mathrm{DC}} < 10^{-1}$ S/m; $0.11 < h < 0.145$ m), which covers all possible solutions of the measurements. It is worth noting that the selected upper limit of the water content is equal to the lower limit of the porosity to ensure that the estimated water content is always smaller than the porosity.

Finally, uncertainty and sensitivity analyses are performed to determine the confidence region of the optimized parameters and the sensitivity of the Green's function with respect to these parameters. For the nonlinear inverse problem, the uncertainty analysis can be carried out using the Monte Carlo method, which requires one to generate many realizations of the parameter sets and therefore takes significant computing resources. In this study, we employed an approximate approach that estimates parameter uncertainty based on the Cramer-Rao inequality (Kool and Parker, 1988; Lambot et al., 2002; Simunek and Hopmans, 2002). For convenience, our calculation is based on the time-domain data, which were transformed from those in the frequency domain by the inverse Fourier transform. According to this approach, the parameter covariance matrix **C** can be computed from the residual error **e** and the Hessian matrix **H**:

$$\mathbf{C} \approx \frac{\mathbf{e}^T e}{n - m}\mathbf{H}^{-1}, \qquad (12)$$

where n and m are the number of measured GPR values and optimized parameters, respectively; the elements H_{ij} of the matrix **H** are defined as

$$H_{ij} = \frac{\partial\phi(\mathbf{b})}{\partial b_i \partial b_j}. \qquad (13)$$

The standard deviation of each optimized parameter b_i can be afterward estimated as an rms of the diagonal elements of the matrix **C**:

$$s_j = \sqrt{C_{jj}} \qquad (14)$$

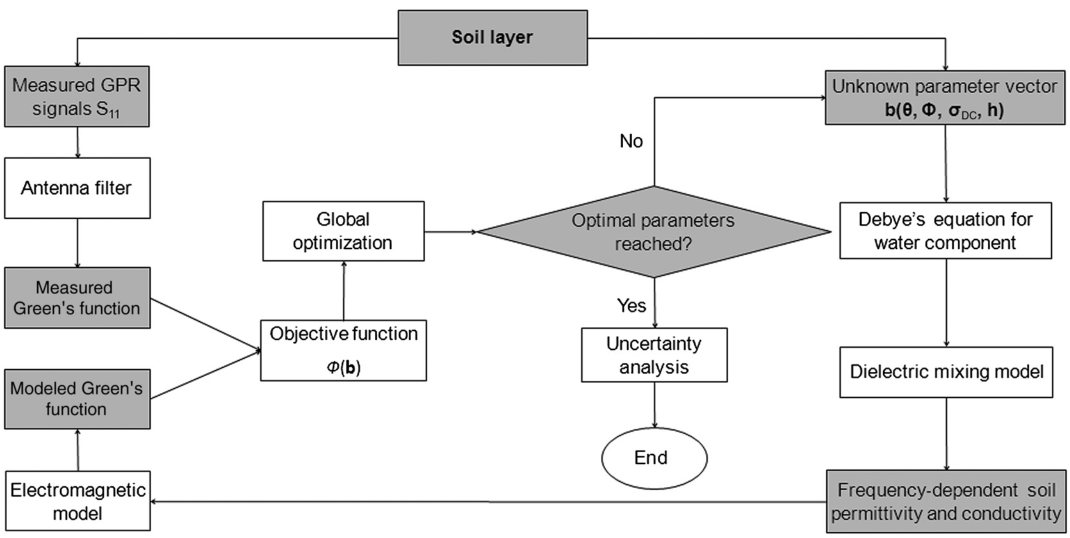

Figure 1. Inverse modeling flowchart to directly obtain the water content from GPR signals.

To evaluate the variation of the Green's function with the optimized parameters and to determine to what extent the parameters can be identified, the sensitivity analysis is a necessity. The sensitivity of a parameter is usually represented by the sensitivity coefficient, which determines the Green's function behavior around a particular point in the parameter space. In this study, we selected the region around the measured values of the porosity, water content, sand layer thickness, and optimized value of the DC conductivity from 11 experiments to analyze the sensitivity. Elements S_{ij} of the sensitivity coefficient matrix **S** are given by

$$S_{ij} = b_j J_{ij}, \tag{15}$$

where **J**,

$$J_{ij} = \frac{\partial \mathbf{G}_{\mathbf{xx}}^{\uparrow}(\mathbf{b}, t_i)}{\partial b_j}, \tag{16}$$

is the Jacobian matrix describing the variation of the Green's function with respect to the parameter b_j at time t_i. Due to the fact that the analytical derivative 16 is difficult to obtain, it is estimated using the forward-finite-difference approximation with a step of parameter $\Delta b_j = 1\% b_j$. To compare the sensitivities of the different parameters, the average sensitivities corresponding to each parameter over the selected time frame (0–10 ns) were calculated as

$$\xi_j = \frac{1}{n} \sum_{i=1}^{n} S_{ij}. \tag{17}$$

It is worth noting that the sensitivity coefficients S_{ij} of the parameters b_j are normalized by b_j so that we can compare the sensitivity of the Green's function to each parameter. The parameter with the higher sensitivity coefficient has a higher chance of being identified.

EXPERIMENTAL RESULTS

Experimental setup

The experiments were conducted in controlled laboratory conditions. The size of the experiment tank was a 2×2-m plane area filled by sand with a porosity of 37.7%. The sand layer was around 13 cm thick. Silicon dioxide (SiO_2) constituted up to 99.16% of the soil materials. With respect to the grain-size distribution, 35.8% of soil grain had a diameter of 500–250 μm, 21.9% of 250–100 μm, 41.4% of 100–50 μm, and 0.90% of smaller than 50 μm. The relative permittivity of the dry sand was 2.64. Tapwater with a DC conductivity of 0.079 S/m was used to put into the sand. For making the soil homogeneous, a concrete mixer was employed to mix the sand sample. After that, the sand surface was leveled to be flat and eliminate the impact of surface roughness. To avoid the vertical heterogeneity of the water content, the GPR measurements were carried out immediately after the soil was mixed and the soil surface was made flat.

The frequency-dependent complex value $S_{11}(\omega)$ was measured sequentially over the range of 1–4.5 GHz with a frequency step of 2 MHz. The antenna had a length of 22 cm and an aperture dimension of 14×24 cm. The virtual source point was 7 cm far away from the antenna aperture inside the antenna (Lambot et al., 2005). We calibrated the VNA at the connection between the antenna feed point and the cable using an open-short-match calibration kit.

Eleven measurements from the dry-to-wet states corresponding to 11 water contents were performed. For each measurement, three sand samples were collected at three locations in the region of the antenna footprint by 250 cm^3-laboratory-made metallic rings with a height of 5 cm and were dried in an oven at 105°C for at least 24 hours to determine the weight of water in the soil sample. The gravimetric water content of each sample was estimated as a ratio of the mass of water and that of the dry sand. Then, the volumetric water content was calculated by multiplying the gravimetric one by the bulk density of the sand. Finally, the volumetric water contents were averaged to obtain the mean value for each experiment.

Table 1 presents the information on the antenna heights, sand-layer thicknesses, and water content for each experiment. As shown in the table, the antenna was situated at heights varying from 25.3 to 32.3 cm above the sand surface, corresponding to a virtual source point situated at 32.3–39.3 cm height. The water content increased from 0.044 to 0.22 cm^3/cm^3 with a standard deviation of 0.0028–0.0091 cm^3/cm^3. It should be noted that the contributions of the horizontal variations to the measurement error were larger than those of vertical variations due to the fact that the vertical variations were averaged over the depth of the metallic ring.

Accuracy of water-content estimation

We selected the frequency range of 1–4.5 GHz for inversion to validate our approach with CRIM and Wang and Schmugge (1980) models. Moreover, for comparison purpose, the approach of Lambot et al. (2005), which assumes a linear relationship between apparent conductivity and frequency, was also applied in this study. Figures 2 and 3 show the measured and modeled Green's functions estimated by CRIM and Wang and Schmugge (1980) mixing models in the frequency and time domains. The WC1 experiment

Table 1. Measured antenna heights, sand thicknesses, and water contents for 11 experiments.

Experiment	Antenna height (m)	Sand thickness (m)	Water content (cm^3/cm^3) Mean	Water content (cm^3/cm^3) Standard deviation
1	0.253	0.131	0.0441	0.0028
2	0.287	0.132	0.0584	0.0029
3	0.318	0.129	0.066	0.0031
4	0.295	0.128	0.0701	0.0091
5	0.31	0.123	0.0787	0.0029
6	0.298	0.131	0.0982	0.0085
7	0.296	0.129	0.107	0.0087
8	0.323	0.136	0.110	0.0062
9	0.321	0.131	0.122	0.0060
10	0.282	0.129	0.148	0.0048
11	0.275	0.130	0.219	0.0036

represents the dry state and WC7 the wet state of sand. In both experiments, the performance of the two models in time and frequency domains was very good. In the frequency domain, the magnitude and phase angle of the modeled Green's function agreed well with those of the measured one (Figures 2b, 2d, 3b, and 3d). The lower agreement was observed at the wet sand (WC7) and high frequencies (greater than around 3.2 GHz).

In the time domain, as we can see in Figures 2a and 3a, the sand surface, PEC, and first-order multiple reflection signals were perfectly reproduced in the first experiment. The differences between measurement and modeling were negligible. The impacts of water on the GPR signals can be seen in Figures 2c and 3c. Although the amplitude of sand-surface reflection signals was nearly the same as that of the WC1 experiment, the amplitude of PEC reflections reduced remarkably (82%) from 76.9 to 14, and we cannot see the multiple reflections from the sand layer in this experiment any more. Thus, the increase of the water content caused considerable losses of GPR signals in the selected frequency range. Comparing the Green's function obtained from the two experiments, we also see that the reflection from the sand surface in the WC1 experiment arrived earlier than that from the WC7 experiment. This is because the antenna in the former experiment was located nearer the sand medium than the later one.

Figure 4 presents the minimum objective functions of 11 water contents achieved by inversion with the three approaches. The figure shows that, in general, the approach of Lambot et al. (2005) provided higher errors compared to our approach, and the gaps seem higher for the wetter conditions. This can be attributed to the fact that the approach of Lambot et al. (2005) assumed a linear dependence of the apparent conductivity with the frequency, whereas our approach accounted for the nonlinear effects. In addition, it can be realized that the disagreement between measurement and model signals of all approaches increased as the water content increased. It might be explained by the more complicated interactions between water-sand and water-water in the sand mixture. Another reason could be the increased discrepancy in the hypothesis

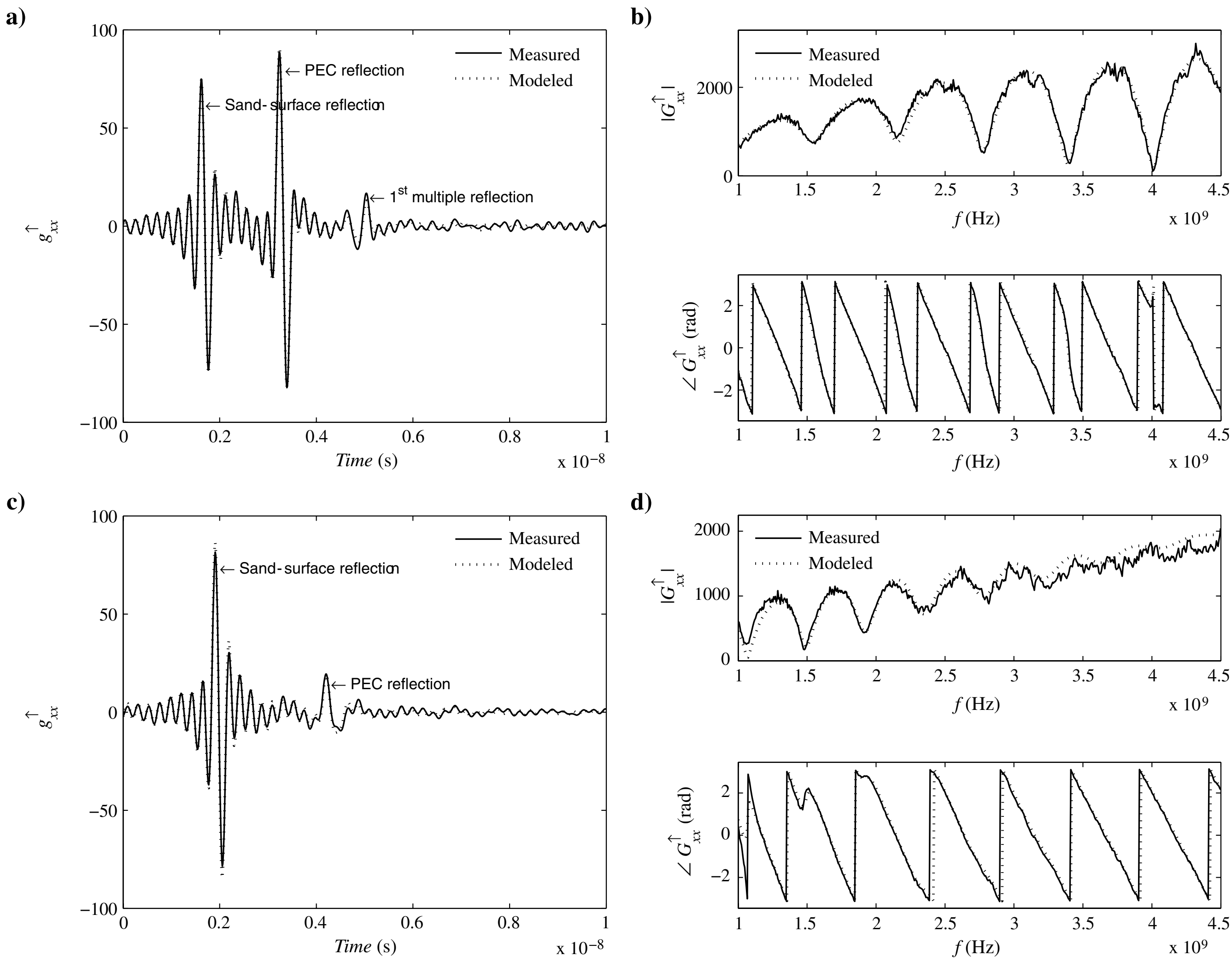

Figure 2. Measured and modeled Green's functions for the WC1 ($\theta = 0.044\ \mathrm{cm^3/cm^3}$) (a and b) and the WC7 ($\theta = 0.11\ \mathrm{cm^3/cm^3}$) (c and d) experiments. The results were obtained by coupling full-wave inversion of GPR signals with CRIM and presented in time (a and c) and frequency (b and d) domains. The time-domain Green's function ($g_{xx}^{\uparrow}$) was obtained by inverse Fourier transform from the Green's function in the frequency domain $G_{xx}^{\uparrow}$.

underlying the GPR model and the experimental medium related to the vertical heterogeneity of the medium with the water content. Although a homogeneous layer with a unique water-content value was assumed in the full-wave GPR model, the soil is naturally wetter toward the base of the experimental tank under the effect of the hydrostatic pressure gradient. This effect is stronger as the sand-water content increases, which makes the homogeneous assumption more violated (see Lambot et al. [2004a] for more detailed analysis on this effect). However, within the time frame to implement our experiments (11–17 minutes) after the soil was mixed homogeneously, this effect is expected not to be very significant. It is worth noting as well that the greater the sand-water content, the greater the reflection at the sand surface and the smaller the reflection at the bottom boundary (PEC). The permittivity (or correlated water content) information tends therefore to come from the surface reflection only, with a decreasing sensitivity to permittivity for increasing permittivity and hence larger uncertainty. The decrease of S/N and lower sensitivity of the water content in the wetter condition also reduces the accuracy of the modeled water content.

The measured and optimized water contents of the approaches are compared in Figure 5. The approach of Lambot et al. (2005) with Topp's model underestimated the water content. For the low and medium water contents, the difference between optimized and measured values were relatively small. However, when the sand became wet, the disagreement between measurement and estimation using this approach was significant. Compared with the Lambot et al. (2005) approach, CRIM and Wang and Schmugge's (1980) mixing models presented more accurate results. The average absolute errors of water-content estimation of these two models were 0.0113 and 0.0126 cm^3/cm^3, respectively, whereas that of Lambot et al.'s (2005) approach was 0.0156 cm^3/cm^3. The correlation coefficients between measured and modeled water contents of our approach (0.984 for Wang and Schmugge's [1980] model and 0.97 for CRIM) were also higher than that of Lambot et al.'s (2005) approach (0.945). There are two main reasons for this fact: (1) More complicated dependence of the permittivity and apparent conductivity are accounted for in the mixing models, and (2) by coupling the mixing models with

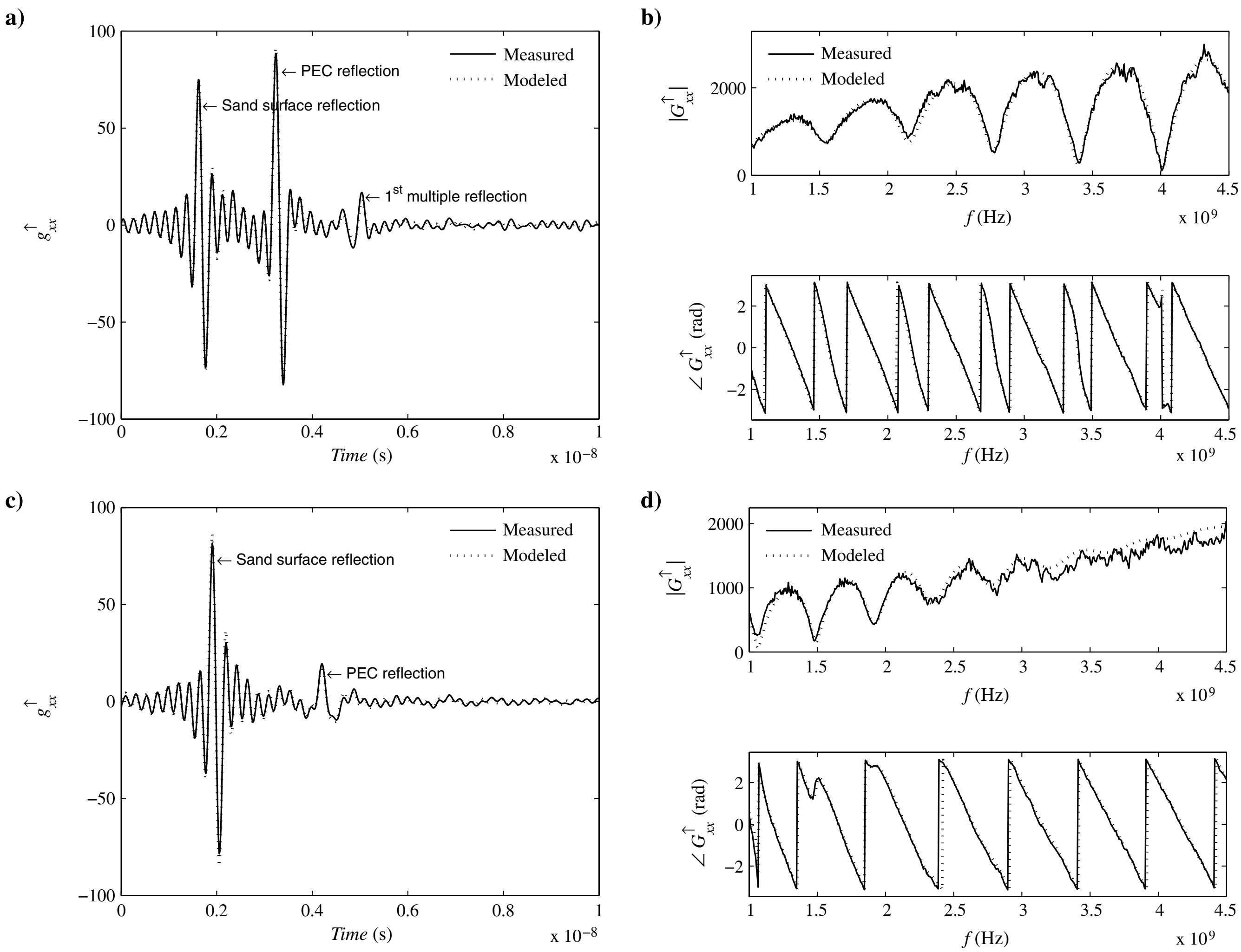

Figure 3. Measured and modeled Green's functions for the WC1 ($\theta = 0.044$ cm^3/cm^3) (a and b) and the WC7 ($\theta = 0.11$ cm^3/cm^3) (c and d) experiments. The results were obtained by coupling full-wave inversion of GPR signals with the mixing model of Wang and Schmugge (1980) and presented in time (a and c) and frequency (b and d) domains. The time-domain Green's function ($g^{\uparrow}_{xx}$) was obtained by inverse Fourier transform from the Green's function in the frequency domain $G^{\uparrow}_{xx}$.

full-wave inversion modeling, sand-water content is directly estimated from GPR signals, whereas the approach of Lambot et al. (2005) indirectly derived this quantity via dielectric permittivity. Of two mixing models, CRIM performed slightly better than Wang and Schmugge's (1980) model for the dry sands, but for the wet sands, the Wang and Schmugge (1980) model's performance was better. Overall, Wang and Schmugge's (1980) model more accurately predicted the water content.

Figure 5 also shows the confidence intervals of the measurements as well as the inversion, which were approximated by their standard deviations. As can be seen from the figure, there is no clear trend in the measurement error. The maximum measurement error was found at the WC4 (0.0091 cm^3/cm^3) and the minimum at the WC1 (0.0028 cm^3/cm^3). This kind of error might be attributed to the heterogeneity of the sand samples at different locations and sampling errors in the horizontal plane. Comparing the confidence intervals of the inversion, we can observe that the confidence intervals of the Lambot et al. (2005) approach are more narrow than those of the mixing models. The reason for this fact is that for the approach of Lambot et al. (2005), we only considered the uncertainty of the inversion. The uncertainty of the transformation from the dielectric permittivity to water content by Topp's equation was not taken into account, whereas the mixing model approach accounted for the uncertainty of water-content estimation. In addition, the uncertainty is greater when the number of parameters to estimate increases. For the two mixing models, the confidence interval of CRIM is broader than that of the Wang and Schmugge (1980) model for all of the measurements.

A very good agreement was also obtained for the thickness of the sand layer. The average relative error of the sand thickness for all estimations was 4.8% and the maximum error was less than 16%. As for the porosity, the optimized results were not as good as those of the water content and thickness of sand layer. The average and maximum relative errors of the estimated porosity for 11 measurements were 19.9% and 36.6%, respectively. This can be explained

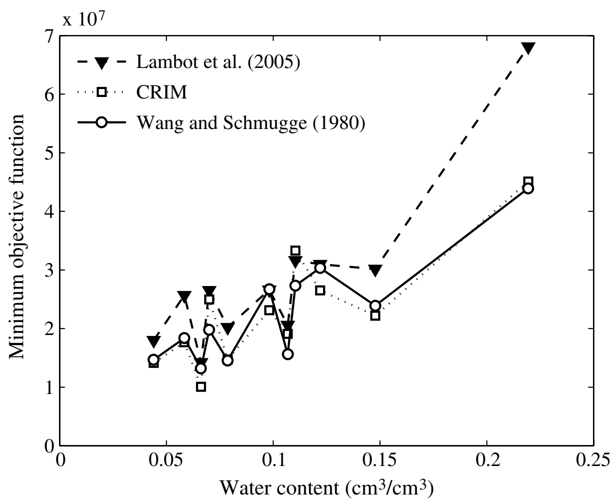

Figure 4. Minimum of the objective function as a function of different water contents. The results obtained by Lambot et al.'s (2005) approach, Wang and Schmugge's (1980) model, and CRIM are compared.

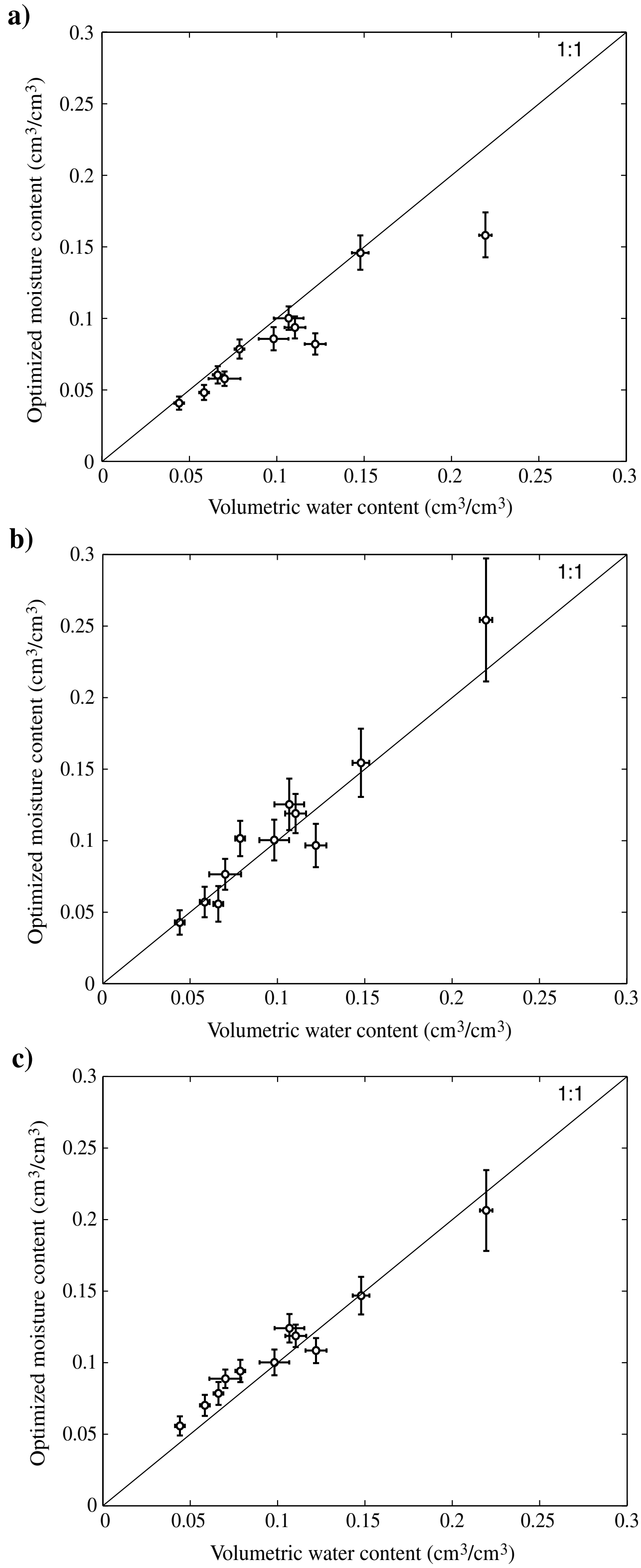

Figure 5. Comparison of measured and optimized water contents. Water contents were estimated by (a) Lambot et al.'s (2005) approach (b) CRIM, and (c) Wang and Schmugge's (1980) model. The horizontal and vertical bars represent the confidence intervals of the measurement and inversion approximated by the standard deviations, respectively.

by the lower sensitivity of the Green's function with respect to the porosity, which is presented in the next section.

Frequency dependence of sand permittivity, apparent conductivity, and attenuation

In this research, the frequency dependence of the geophysical properties was considered in two different ways. First, the sand-water content was estimated by coupling the full-wave inversion of GPR signals with the mixing models over the entire frequency range (1–4.5 GHz). The dielectric permittivity and apparent conductivity of the sand mixture at each frequency were afterward obtained back from the water content by using mixing models. Second, the entire frequency range was divided into seven successive subfrequency bands with steps of 400 MHz (1.0–1.4, 1.4–1.8, 1.8–2.2, 2.2–2.8, 2.8–3.2, 3.2–3.8, and 3.8–4.2 GHz). In each

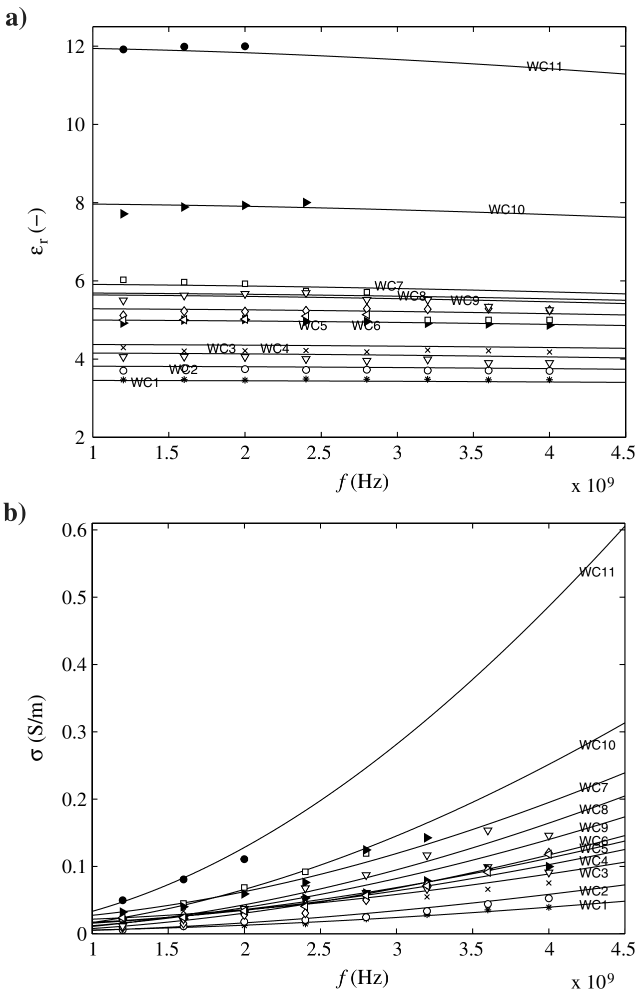

Figure 6. (a) The change of the sand relative permittivity and (b) apparent conductivity versus the frequency of different water contents. The solid line presents the outcomes extracted from coupling Wang and Schmugge's (1980) mixing model with full-wave GPR signal inversion in the entire frequency range (1.0–4.5 GHz). Markers represent the outcomes obtained by full-wave GPR signal inversion in subsequent frequency bands (1.0–1.4, 1.4–1.8, 1.8–2.2, 2.2–2.8, 2.8–3.2, 3.2–3.8, and 3.8–4.2 GHz).

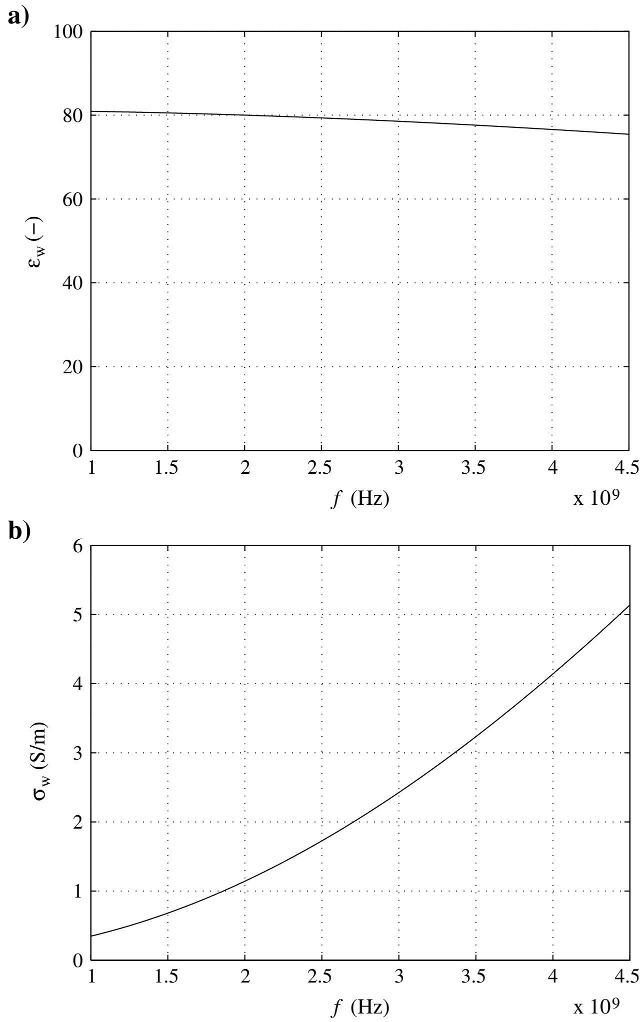

Figure 7. (a) Dielectric permittivity and (b) apparent conductivity of water computed by the Debye model (Debye, 1929) at the frequency range of 1–4.5 GHz.

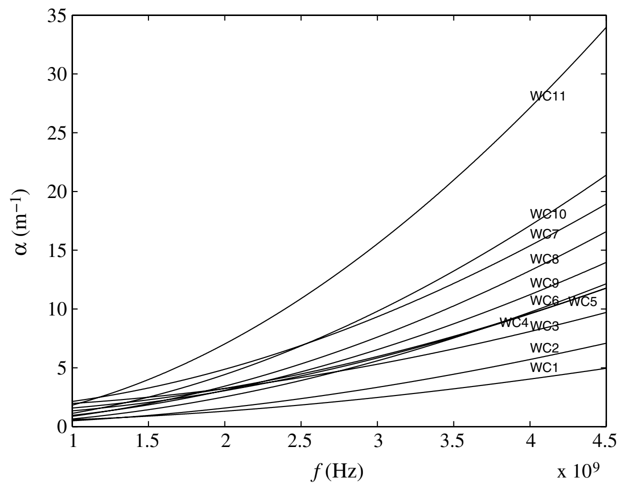

Figure 8. Attenuation coefficient as a function of the frequency at different states of sand moisture. The calculation is based on the mixing model of Wang and Schmugge (1980).

subband, the dielectric permittivity and apparent conductivity were assumed to be constant and were found by inversion of GPR signals. In this case, the optimized parameter vector was $b = [\varepsilon_r, \sigma, h]$. Figure 6 shows the permittivity and apparent conductivity estimated by the two approaches as a function of the frequency for 11 water contents. The mixing model used in this case was Wang and Schmugge's (1980) model. The limited information for inversion of the short subbands sometimes caused several unrealistic optimal values, which are not shown in the figure. Figure 6a implies that the permittivity slightly reduces with increasing frequency in the selected frequency range and the dry soil decreases more slowly than the wet soil. This can be explained by observing Figure 7a, which shows the dependence of the dielectric permittivity of water on frequency by the Debye equation in our selected frequency range. The figure indicates that the water permittivity slowly decreases from about 80.9 at a frequency of 1 GHz to 75.4 at a frequency of 4.5 GHz.

Similar to the permittivity, there was good agreement for the apparent conductivities between the two approaches (Figure 6b). The gaps between them became slightly larger for the high water contents. Because the sand became wetter, the radar waves were more absorbed, which caused the information from reflected signals in the subfrequency bands to be insufficient for the inversion. The figure also shows that the apparent conductivity rises exponentially with the frequency, and the rising magnitude increases when the sand is wetter. These trends imply that the energy is lost considerably with increasing frequency and water content. The same trends were also observed when CRIM was adopted. Again, the dielectric losses of the water component are the main factor that leads to the frequency dependence of the apparent conductivity. As shown in Figure 7b, the apparent conductivity of water rapidly grows from less than 0.35 S/m to greater than 5 S/m as the frequency increases from 1 to 4.5 GHz.

Figure 8 plots the attenuation coefficient versus frequency for 11 water-content measurements. The relationship between this value and the apparent conductivity and permittivity is given by

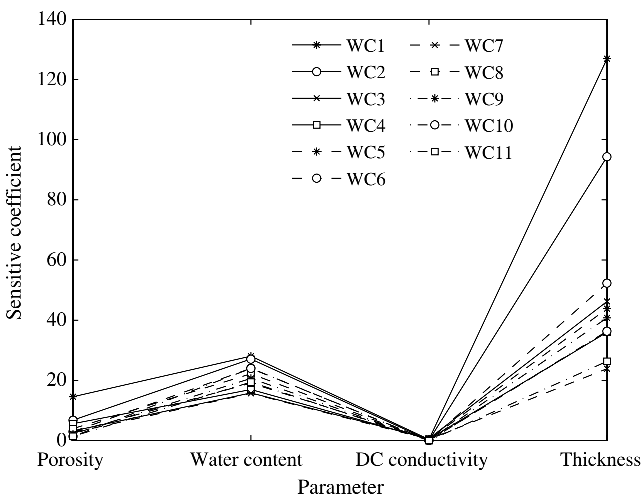

Figure 9. Sensitive coefficients of the porosity, water content, DC conductivity, and sand-layer thickness for 11 measurements. Our results are based on the mixing model of Wang and Schmugge (1980).

$$\alpha = \frac{1}{2}\sigma\sqrt{\frac{\mu}{\varepsilon_0\varepsilon_r}}, \tag{18}$$

where μ is the magnetic permeability of the medium, which is assumed to be equal to that of the free space ($\mu = \mu_0 = 1.25 \times 10^{-6}$ H/m). The equation indicates that the attenuation is proportional to the apparent conductivity and inversely proportional to the permittivity. The figure shows that the variation trend of the attenuation with the frequency is similar to that of the apparent conductivity, indicating that the relationship between the attenuation and the frequency is strongly influenced by the relationship between the apparent conductivity and the frequency. However, if we observe more carefully, especially for the higher-water-content cases, we can see that the slope of the attenuation-frequency relation is slightly steeper due to the slight reduction of the permittivity with the frequency.

UNCERTAINTY ANALYSIS

Figure 9 presents the sensitive coefficients of the optimized parameters for the 11 measurements. The results are calculated based on the mixing model of Wang and Schmugge (1980). There is a consistent trend in the sensitivity of the Green's function in response to the parameters for all of the measurements. The Green's function is most sensitive to the sand thickness, especially for the dry measurements. The sensitive coefficient is up to about 126.9 and 94.3 and for the WC1 and WC2, respectively. The Green's function is also relatively sensitive to the variation of the water content. The sensitive coefficients for the water content vary in the range of 15.7–28.1, which are higher than those for the porosity (1.4–14.5). This explains the less-accurate estimated porosity compared with the sand-layer thickness and water content. As for the DC conductivity (the model-derived value is less than 0.02 S/m in all experiments), the figure shows that the Green's function is insensitive to this parameter, with the sensitive coefficients of all measurements lower than 0.7. Similar trends were also found in the results of the CRIM model.

DISCUSSION

The approach was successfully validated for sandy soil. However, in reality, soil texture is very complex. Further research will focus on the application of the integrated approach for other soil types and, in particular, clay, in which relaxation effects are more complex due to the interactions between the soil and water molecules. Given that restricted rotation of water bound to clay minerals is a source of frequency dispersion in GPR frequency in addition to free water, the effects of the sand and clay contents on the soil's electrical properties are indirectly accounted for via the wilting point (equation 8) and transition moisture (equation 9) of Wang and Schmugge's (1980) mixing model. By investigating the type of soil sample, we can take into account the variation of the soil complex permittivity with the soil type. The complex dielectric permittivity of bound water, with its own relaxation frequency, should be used instead of the real one, such as that done in this study.

In real field applications, there is no PEC as the bottom boundary condition. In that case, less energy is backscattered, depending on the layer contrasts, and the information content in the radar data is therefore decreased. The technique was successfully applied in field conditions for surface soil-moisture mapping (Weihermüller et al., 2007; Minet et al., 2011), and up to two layers could be reconstructed (Lambot et al., 2004b; Minet et al., 2011). If the main interest is the very thin surface soil layer of the subsurface, the soil layer can be simulated by a homogeneous half-space below the air layer. For the case that a soil-moisture profile is preferred, one suggestion is to apply the water-retention curve developed by van Genuchten (1980) to model the water-content variation along a soil column constrained by the soil moisture at the top and the bottom of the soil column. The soil-moisture values of the top and bottom layers are related to the complex permittivities by the mixing model and can be estimated by our full-wave inversion model. These implementations will increase the number of unknown parameters, which may affect the well-posedness of the inverse problems dealt with. Thus, a sensitivity analysis should be done to remove the insensitive variables. In addition, a general prior knowledge on the soil texture and structure is important to take a reasonable constraint the parameter space to support the global optimization searching.

CONCLUSION

By coupling the dielectric mixing models of soil mixture and the full-wave inversion of zero-offset off-ground radar signals, we achieved two main improvements to enhance the accuracy of water-content estimation. First, the frequency dependence of the apparent permittivity and conductivity was taken into account. Second, unlike the currently adopted methods, we could directly derive the water content of soil from inversion of GPR signals without the need for a specific relationship. Furthermore, in this study, we did not need to determine a priori specific soil porosity when the dielectric mixing models of soil were used. With these improvements, together with advantages of the full-wave inversion model, our approach was successfully validated for the experimental measurements above a sandy soil layer in laboratory conditions. The estimated Green's functions were well fitted with those of the measurements, leading to a very high accuracy of the estimated water content. The average absolute errors obtained by the approach were less than 0.013 cm^3/cm^3 and the correlation coefficients were greater than 0.97. Comparing the two mixing models, the water contents estimated by the CRIM were slightly more accurate than those of the Wang and Schmugge model for the dry sands but were less accurate for the wet sands. In general, performance of the Wang and Schmugge model was better. An accurate estimation was also obtained for the sand-layer thickness, with the average relative error less than 5%, but less accurate for the porosity, with the average relative error of about 20%. The results also pointed out that for sandy soil, the permittivity is approximately independent of frequency and the apparent conductivity is exponentially dependent on frequency. The sensitivity analysis pointed out that the Green's function is the most sensitive to the variation of the water content and sand-layer thickness but insensitive to the DC conductivity. This is the reason for the very accurate estimation of the two parameters.

ACKNOWLEDGMENTS

This work was supported by the European Commission under the 7th Framework Programme for Research and Technological Development (DIGISOIL project), the FNRS (Fonds National de la Recherche Scientifique, Belgium), and the Université Catholique de Louvain (Belgium).

REFERENCES

Bradford, J. H., and J. C. Deeds, 2006, Ground-penetrating radar theory and application of thin-bed offset-dependent reflectivity: Geophysics, **71**, no. 3, K47–K57, doi: 10.1190/1.2194524.

Chanzy, A., A. Tarussov, F. Bonn, and A. Judge, 1996, Soil water content determination using digital ground-penetrating radar: Soil Science Society of America Journal, **60**, 1318–1326, doi: 10.2136/sssaj1996.03615995006000050005x.

Debye, P., 1929, Polar molecules: Reinhold.

Deparis, J., and S. Garambois, 2009, On the use of dispersive APVO GPR curves for thin-bed properties estimation: Theory and application to fracture characterization: Geophysics, **74**, no. 1, J1–J12, doi: 10.1190/1.3008545.

Dirksen, C., and S. Dasberg, 1993, Improved calibration of time domain reflectometry soil water content measurements: Soil Science Society of America Journal, **57**, 660–667, doi: 10.2136/sssaj1993.03615995005700030005x.

Dobson, M. C., F. F. Ulaby, M. T. Hallikainen, and M. A. El-Rayes, 1985, Microwave dielectric behavior of wet soil — Part II: Dielectric mixing models: IEEE Transactions on Geoscience and Remote Sensing, **GE-23**, 35–46, doi: 10.1109/TGRS.1985.289498.

Galagedara, L. W., J. D. Redman, G. W. Parkin, A. P. Annan, and A. L. Endres, 2005, Numerical modeling of GPR to determine the direct ground wave sampling depth: Vadose Zone Journal, **4**, no. 4, 1096–1106, doi: 10.2136/vzj2004.0143.

Gorriti, A. G., 2004, Electric characterization of sands with heterogeneous saturation distribution: Ph.D. thesis, Delft University of Technology.

Greaves, R. J., D. P. Lesmes, J. M. Lee, and M. N. Toksov, 1996, Velocity variations and water content estimated from multi-offset, ground-penetrating radar: Geophysics, **61**, 683–695, doi: 10.1190/1.1443996.

Gregoire, C., and F. Hollender, 2004, Discontinuity characterization by the inversion of the spectral content of ground penetrating radar (GPR) reflections — Application of the Jonscher model: Geophysics, **69**, 1414–1424, doi: 10.1190/1.1836816.

Heimovaara, T. J., 1994, Frequency domain analysis of time domain reflectometry waveforms: 1. Measurement of the complex dielectric permittivity of soils: Water Resources Research, **30**, 189–199, doi: 10.1029/93WR02948.

Hilhorst, M. A., C. Dirksen, F. W. H. Kampers, and R. A. Feddes, 2001, Dielectric relaxation of bound water versus soil matric pressure: Soil Science Society of America Journal, **65**, 311–314, doi: 10.2136/sssaj2001.652311x.

Huisman, J. A., S. S. Hubbard, J. D. Redman, and A. P. Annan, 2003, Measuring soil water content with ground penetrating radar: A review: Vadose Zone Journal, **2**, no. 4, 476–491, doi: 10.2113/2.4.476.

Huisman, J. A., C. Sperl, W. Bouten, and J. M. Verstraten, 2001, Soil water content measurements at different scales: Accuracy of time domain reflectometry and ground penetrating radar: Journal of Hydrology, **245**, 48–58, doi: 10.1016/S0022-1694(01)00336-5.

Huyer, W., and A. Neumaier, 1999, Global optimization by multilevel coordinate search: Journal of Global Optimization, **14**, 331–355, doi: 10.1023/A:1008382309369.

Klein, L. A., and C. T. Swift, 1977, An improved model for the dielectric constant of sea water at microwave frequencies: IEEE Transactions on Antennas and Propagation, **25**, 104–111, doi: 10.1109/TAP.1977.1141539.

Kool, J. B., and J. C. Parker, 1988, Analysis of the inverse problem for transient unsaturated flow: Water Resources Research, **24**, 817–830, doi: 10.1029/WR024i006p00817.

Lambot, S., F. Hupet, M. Javaux, and M. Vanclooster, 2004a, Laboratory evaluation of a hydrodynamic inverse modeling method based on water content data: Water Resources Research, **40**, W03506, doi: 10.1029/2003WR002641.

Lambot, S., M. Javaux, F. Hupet, and M. Vanclooster, 2002, A global multilevel coordinate search procedure for estimating the unsaturated soil hydraulic properties: Water Resources Research, **38**, 1224–1239, doi: 10.1029/2001WR001224.

Lambot, S., J. Rhebergen, I. van den Bosch, E. C. Slob, and M. Vanclooster, 2004b, Measuring the soil water content profile of a sandy soil with an off-ground monostatic ground penetrating radar: Vadose Zone Journal, **3**, no. 4, 1063–1071, doi: 10.2113/3.4.1063.

Lambot, S., E. C. Slob, I. van den Bosch, B. Stockbroeckx, and M. Vanclooster, 2004c, Modeling of ground-penetrating radar for accurate characterization of subsurface electric properties: IEEE Transactions on Geoscience and Remote Sensing, **42**, 2555–2568, doi: 10.1109/TGRS.2004.834800.

Lambot, S., E. Slob, and H. Vereecken, 2007, Fast evaluation of zero-offset Green's function for layered media with application to ground-penetrating radar: Geophysical Research Letters, **34**, L21405, doi: 10.1029/2007GL031459.

Lambot, S., I. van den Bosch, B. Stockbroeckx, P. Druyts, M. Vanclooster, and E. Slob, 2005, Frequency dependence of the soil electromagnetic properties derived from ground-penetrating radar signal inversion: Subsurface Sensing Technologies and Applications, **6**, 73–87, doi: 10.1007/s11220-005-4228-x.
Lambot, S., L. Weihermüller, J. A. Huisman, H. Vereecken, M. Vanclooster, and E. C. Slob, 2006, Analysis of air-launched ground-penetrating radar techniques to measure the soil surface water content: Water Resources Research, **42**, W11403, doi: 10.1029/2006WR005097.
Lane, J. A., and J. A. Saxton, 1952, Dielectric dispersion in pure polar liquids at very high radio frequencies. III. The effect of electrolytes in solution: Proceedings of the Royal Society of London A, **214**, 531–545, doi: 10.1098/rspa.1952.0187.
Lesmes, D. P., and S. P. Friedman, 2005, Relationships between the electrical and hydrogeological properties of rocks and soils, *in* Y. Rubin, and S. S. Hubbard eds., Hydrogeophysics: Springer, 87–128.
Looyenga, H., 1965, Dielectric constants of heterogeneous mixtures: Physica (Amsterdam), **31**, 401–406, doi: 10.1016/0031-8914(65)90045-5.
Minet, J., A. Wahyudi, P. Bogaert, M. Vanclooster, and S. Lambot, 2011, Mapping shallow soil moisture profiles at the field scale using full-waveform inversion of ground penetrating radar data: Geoderma, **161** no. 3–4, 225–237, doi: 10.1016/j.geoderma.2010.12.023.
Nelder, J. A., and R. Mead, 1965, A simplex method for function minimization: The Computer Journal, **7**, 308–313, doi: 10.1093/comjnl/7.4.308.
Redman, J. D., J. L. Davis, L. W. Galagedara, and G. W. Parkin, 2002, Field studies of GPR air launched surface reflectivity measurements of soil water content: Proceedings of the 9th International Conference on Ground Penetrating Radar, SPIE, 156–161, doi: 10.1117/12.462256.
Robinson, D. A., A. Binley, N. Crook, F. D. Day-Lewis, T. P. A. Ferre, V. J. S. Grauch, R. Knight, M. Knoll, V. Lakshmi, R. Miller, J. Nyquist, L. Pellerin, K. Singha, and L. Slater, 2008, Advancing process-based watershed hydrological research using near-surface geophysics: A vision for, and review of, electrical and magnetic geophysical methods: Hydrological Processes, **22**, 3604–3635, doi: 10.1002/hyp.v22:18.
Robinson, D. A., S. B. Jones, J. M. Wraith, D. Or, and S. P. Friedman, 2003, A review of advances in dielectric and electrical conductivity measurement in soils using time domain reflectometry: Vadose Zone Journal, **2**, no. 4, 444–475, doi: 10.2113/2.4.444.
Roth, K., R. Schulin, H. Flühler, and W. Attinger, 1990, Calibration of time domain reflectometry for water content measurement using a composite dielectric approach: Water Resources Research, **26**, no. 10, 2267–2273, doi: 10.1029/WR026i010p02267.
Saarenketo, T., 1998, Electrical properties of water in clay and silty soils: Journal of Applied Geophysics, **40**, 73–88, doi: 10.1016/S0926-9851(98)00017-2.
Shutko, A. M., and E. M. Reutov, 1982, Mixture formulas applied in estimation of dielectric and radiative characteristics of soils and grounds at microwave frequencies: IEEE Transactions on Geoscience and Remote Sensing, **20**, 29–32, doi: 10.1109/TGRS.1982.4307516.
Simunek, J., and J. Hopmans, 2002, Parameter optimization and nonlinear fitting, *in* J. H. Topp, and G. C. Dane, eds., Methods of soil analysis: Part 4 — Physical methods: Soil Science Society of America, 139–157.
Slob, E., M. Sato, and G. Olhoeft, 2010, Surface and borehole ground-penetrating-radar developments: Geophysics, **75**, no. 5, A103–A120, doi: 10.1190/1.3480619.
Stogryn, A., 1970, The brightness temperature of a vertically structured medium: Radio Science, **5**, 1397–1406, doi: 10.1029/RS005i012p01397.
Strobbia, C., and G. Cassiani, 2007, Multilayer ground-penetrating radar guided waves in shallow soil layers for estimating soil water content: Geophysics, **72**, no. 4, J17–J29, doi: 10.1190/1.2716374.
Topp, G. C., J. L. Davis, and A. P. Annan, 1980, Electromagnetic determination of soil water content: Measurements in coaxial transmission lines: Water Resources Research, **16**, 574–582, doi: 10.1029/WR016i003p00574.
van der Kruk, J., R. W. Jacob, and H. Vereecken, 2010, Properties of precipitation-induced multilayer surface waveguides derived from inversion of dispersive TE and TM GPR data: Geophysics, **75**, no. 4, WA263–WA273, doi: 10.1190/1.3467444.
van Genuchten, M. T., 1980, A closed-form equation for predicting the hydraulic conductivity of unsaturated soils: Soil Science Society of America Journal, **44**, 892–898, doi: 10.2136/sssaj1980.03615995004400050002x.
Vereecken, H., J. A. Huisman, H. Bogena, J. Vanderborght, J. A. Vrugt, and J. W. Hopmans, 2008, On the value of soil moisture measurements in vadose zone hydrology: A review: Water Resources Research, **44**, W00D06, doi: 10.1029/2008WR006829.
Wang, J. R., and T. J. Schmugge, 1980, An empirical model for the complex dielectric permittivity of soils as a function of water content: IEEE Transactions on Geoscience and Remote Sensing, **GE-18**, 288–295, doi: 10.1109/TGRS.1980.350304.
Weihermüller, L., J. A. Huisman, S. Lambot, M. Herbst, and H. Vereecken, 2007, Mapping the spatial variation of soil water content at the field scale with different ground penetrating radar techniques: Journal of Hydrology, **340**, no. 3–4, 205–216, doi: 10.1016/j.jhydrol.2007.04.013.
West, L. J., K. Handley, Y. Huang, and M. Pokar, 2003, Radar frequency dielectric dispersion in sandstone: Implications for determination of moisture and clay content: Water Resources Research, **39**, 1026–1038, doi: 10.1029/2001WR000923.
Woodhead, I. M., G. D. Buchan, J. H. Christie, and K. Irie, 2003, A general dielectric model for time domain reflectometry: Biosystems Engineering, **86**, 207–216, doi: 10.1016/S1537-5110(03)00131-4.